

A billion years of evolution manifest in nanosecond protein dynamics

Philipp J. Heckmeier^{*,1}, Jeannette Ruf¹, Charlotte Rochereau², and Peter Hamm¹

¹*Department of Chemistry, University of Zurich, Zurich, Switzerland*

²*Department of Systems Biology, Columbia University, USA*

*philipp.heckmeier@chem.uzh.ch

(Dated: 13th September 2023)

Protein dynamics form a critical bridge between protein structure and function^{1,2}, yet the impact of evolution on ultrafast processes inside proteins remains enigmatic. This study delves deep into nanosecond-scale protein dynamics of a structurally and functionally conserved protein across species separated by almost a billion years³⁻⁵, investigating ten homologs in complex with their ligand. By inducing a photo-triggered destabilization of the ligand inside the binding pocket^{6,7}, we resolved distinct kinetic footprints for each homolog via transient infrared spectroscopy^{8,9}. Strikingly, we found a cascade of rearrangements within the protein complex which manifest in three discrete time points of dynamic activity, conserved over hundreds of millions of years within a narrow window. Among these processes, one displays a subtle temporal shift correlating with evolutionary divergence, suggesting reduced selective pressure in the past. Our study not only uncovers the impact of evolution on molecular processes in a specific case, but has also the potential to initiate a novel field of scientific inquiry within molecular paleontology, where species are compared and classified based on the rapid pace of protein dynamic processes; a field which connects the shortest conceivable time scale in living matter (10^{-9} s) with the largest ones (10^{16} s).

MAIN

Proteins exist as dynamic ensembles, rather than being rigid and static entities. They constantly undergo rearrangements, folding-, and unfolding processes on a nanosecond time scale^{2,6,7,10}. Understanding this dynamic nature is essential to comprehending their function. As protein dynamics serve as the crucial link between structure and function¹, their experimental investigation has predominantly focused on individual protein examples, providing insights into specific¹¹⁻¹³, often intrinsically disordered cases¹⁴⁻¹⁶. Surprisingly, protein dynamics within a group of closely related proteins, such as a family of homologs, have rarely been experimentally explored, and if so, in the slow-paced millisecond-second regime¹⁶⁻¹⁸ where rapid fluctuations of conformational adaptations are not resolved. Consequently, little is known about whether structural homologs display conserved ultrafast protein dynamics throughout evolution. How may nano-scale protein dynamics evolve over hundreds of million years within a protein family?

Revealing the rapid dynamic processes within proteins requires the use of an appropriate toolkit. Thus far, the conservation of protein structures has been primarily observed through structure comparison using X-ray crystallography¹⁹⁻²². X-ray crystallography provides valuable insights with a predominantly static view of proteins, but lacks the mechanistic intricacies that define their dynamics. As an alternative approach, NMR spectroscopy excels at resolving small conformational differences and dynamics in equilibrium^{11,16,17,23}, yet it falls short in recording non-equilibrium processes.

In contrast, infrared spectroscopy is sensitive to subtle differences in protein conformations and is a power-

ful tool to temporally resolve fast dynamical processes within proteins^{8,9}. In combination with an phototrigger, this technique enables the initiation and monitoring of sequential destabilization within a protein complex, with a temporal resolution as fast as a picoseconds^{6,7,24,25}. The key challenge lies in investigating the specific time points at which certain processes occur, in order to resolve the influence of evolution on molecules that are inherently dynamic and exhibit fluent transitions between conformational states.

MCL-1: A PRIME EXAMPLE OF CONSERVATION

This study is concerned with the protein myeloid cell leukemia 1 (MCL-1), a member of the BCL-2 protein family, which plays a crucial role as a key regulator of apoptosis, the programmed cell death^{3,29}. It is found not only in humans, but also in a diverse range of metazoan organisms^{4,30}. Functioning as an anti-apoptotic protein, MCL-1 interacts promiscuously with pro-apoptotic factors through α -helical domains known as BCL-2 homology domain 3 (BH3)^{4,29,31,32}, e.g. the BH3 domain of the pro-apoptotic protein PUMA^{26,33} (Fig. 1a). Homologs of this protein family have been identified in all vertebrates and even in more distantly related species such as sponges³⁴ and *Cnidaria*³⁵, whose last common ancestor with *Homo sapiens* existed over 700 million years ago⁵.

We selected ten MCL-1 homologs (Fig. 1b) from species, whose last common ancestors with *Homo sapiens* are distributed equidistantly on an evolutionary time axis up to a billion years from present day to the past. We opted for a horizontal approach by comparing se-

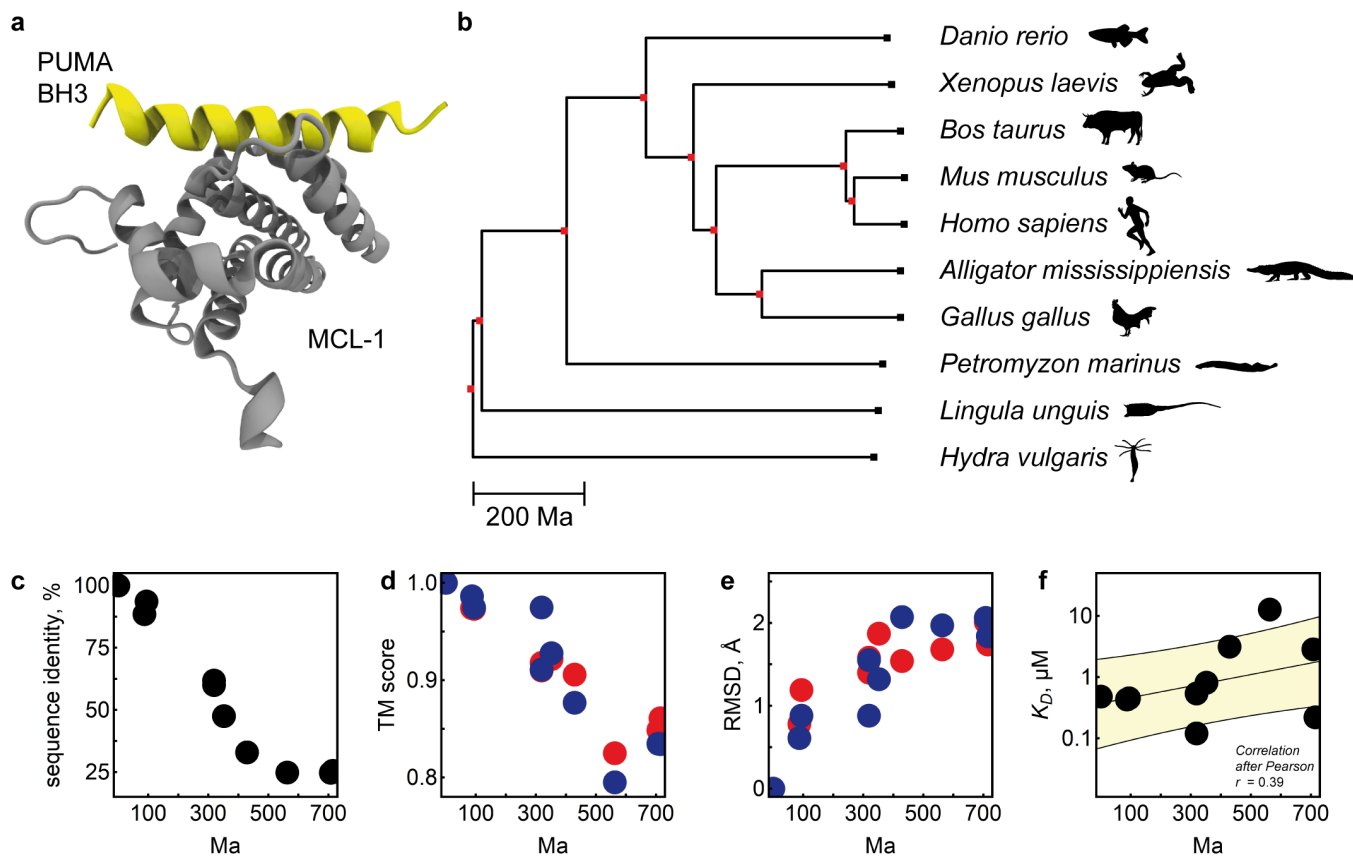


FIG. 1. Structure and function of MCL-1 is conserved. (a) NMR structure of MCL-1 (grey) complexed with PUMA BH3 (yellow) (PDB: 2roc)²⁶. (b) Phylogeny of ten species whose MCL-homologs were selected for this study. The phylogeny and the corresponding evolutionary divergence time in million years (Ma) were taken from TimeTree5 and cover the current state of science (July 2023)⁵. (c) Sequence identity of all investigated MCL-1 homologs (compared to *H. sapiens*) against evolutionary divergence time of the corresponding species. (d,e) Structural similarity between MCL-1 homologs (compared to *H. sapiens*), predicted with AlphaFold²⁷ (blue) and RosettaFold²⁸ (red). (f) MCL-1 homolog binding free energy for the PUMA BH3 peptide, plotted against the evolutionary divergence time. Yellow, linear fit \pm standard deviation. The Pearson correlation coefficient $r = 0.39$ indicates that the binding free energy correlates weakly with evolutionary divergence time.

quences of currently living species, as opposed to a vertical approach involving the reconstruction of ancestral proteins^{36,37}. Besides *Homo sapiens*, we included *Mus musculus*, *Bos taurus*, *Gallus gallus*, *Alligator mississippiensis*, *Xenopus laevis*, *Danio rerio*, a *Petromyzon marinus* candidate³⁸, *Lingula unguis*, and *Hydra vulgaris*.

Before exploring the protein dynamics for this homolog selection, our objective was to unequivocally establish the conservation of both the structure and function of MCL-1. By comparing the amino acid sequences of the homologs to their human equivalent, we found that sequence identity dramatically decreased as a function of evolutionary divergence (Fig. 1c), approaching a level of saturation at 25% where homology becomes challenging to detect³⁹. The conserved amino acid residues are mostly associated with the canonical binding groove (Extended Data Fig. 1a), consistent with the prevailing scientific perspective⁴⁰, or are localized at the hydrophobic core of the protein. As solely the human and murine

homologs bear experimentally acquired structures (e.g. PDB: 6QFM, 2ROC), we used two structure prediction models, AlphaFold²⁷ and RosettaFold²⁸, to compute the structures for the remaining homologs (Extended Data Fig. 1b). In comparison to their experimental equivalents, we found conserved topologies (TM scores $\geq 80\%$ ^{41,42}, Fig. 1d) and only small spatial differences between the predicted protein backbone (RMSD ≤ 2.5 Å, Fig. 1e). A subtle correlation between inferior structural conservation and increased divergence time became visible. Nevertheless, the predictions show that, although sequences might differ strikingly, MCL-1 structure did not substantially change over a long evolutionary time scale⁴³.

The primary function of MCL-1, i.e., the ability to strongly bind the BH3 domain in its binding pocket, which makes it a pivotal anti-apoptotic regulator, is also conserved. We experimentally determined MCL-1's binding affinity for a uniform PUMA BH3 ligand (bearing mu-

tations for crosslinking, see extended Data Fig. 2), with K_D values ranging from 100 nM to 1 μ M for most homologs. We detected a weak correlation of $\log K_D$, which refers to the binding free energy, with evolutionary divergence time (Fig. 1f). Notably, homologs from both *Hydra vulgaris* and *Homo sapiens*, separated by an evolutionary distance of over 700 million years, bound the same ligand with comparable affinities ($K_{D,Hydra} = 220$ nM, $K_{D,Homo} = 480$ nM). Given its critical function as a 'life/death switch'³ in numerous animal species, this result confirms that MCL-1 indeed exhibits a high degree of structural and functional conservation, manifesting in minor differences at the molecular level.

MCL-1's role as a prime example of structural and functional conservation raises the question of whether the dynamics of the protein are also conserved. Are the nanosecond processes occurring in human MCL-1 also present in *Hydra vulgaris* MCL-1?

CONSERVATION OF PROTEIN DYNAMICS

To examine the impact of extremely slow evolutionary processes on the fast-paced protein dynamics of MCL-1, we used transient infrared spectroscopy in combination with a photoswitchable azobenzene moiety that is covalently bound to the PUMA BH3 ligand (Fig. 2a, Methods). In its *cis*-state, the crosslinked photoswitch additionally stabilizes the ligand inside the binding pocket (Extended Data Fig. 2m). Conversely, the light-induced transition from the *cis*- to the *trans* configuration leads to a reduction in α -helicity (Extended Data Fig. 2n), indicating a destabilization of PUMA BH3.

Considering a time frame from pico- to microseconds²⁵, we studied the protein dynamics in a pump-probe experiment where the *cis*-to-*trans* isomerization of the photoswitch is triggered by an ultrashort UV/VIS laser pulse at 420 nm and the protein vibrational spectrum is probed in the mid infrared region around 1650 cm^{-1} (Fig. 2b). In this spectral region, C=O stretch vibrations of the protein backbone can be observed. Negative (blue) and positive (red) absorption changes serve as indicator for structural alterations⁴⁶. We obtained homolog-specific kinetic footprints for the ten investigated species (Extended Data Fig. 3, exemplified for *M. musculus* in Fig. 2c). Analogous to fossil footprints – the paleontologic counterpart –, the kinetic footprints display comparable elements. All of them are similarly shaped, displaying a blue shift of a band at 1645 cm^{-1} , which reveals a negative bleach towards a new (positive) band at 1675 cm^{-1} (Fig. 2c, triangle). The signal appears within the low nanosecond time frame for all of the homologs and can be attributed to α -helix unfolding^{7,9,47}. More strikingly, the kinetic footprints exhibit diverging, species-specific details, which are particularly well visible for the spectral feature between 1655 cm^{-1} and 1685 cm^{-1} (Fig. 2c, circle), and a late negative feature at 1620 cm^{-1} forming at around 100 ns

(Fig. 2c, square). The first-mentioned feature (circle) is especially pronounced for mammalian/avian/reptilian homologs (Extended Data Fig. 3a-e), but loses its distinct appearance more and more for species with higher evolutionary divergence (*P. marinus*, *L. unguis*, *H. vulgaris* (Extended Data Fig. 3h-j), displaying a solitary, less emphasized maximum at 1660 cm^{-1} . Furthermore, the kinetic footprints of the non-*Gnathostomata* *P. marinus*, *L. unguis*, and *H. vulgaris*, lack the late negative feature at 1620 cm^{-1} .

All kinetic footprints are dominated by three phases of dynamic activity, an early-, mid-, and late phase, where the intensity of spectral features grows or decreases significantly (exemplified for *M. musculus* in Fig. 2d, for all other species in Extended Data Fig. 4). To fathom these three dynamic processes and their corresponding time constants, we analyzed the kinetic footprints with global multiexponential fitting (Fig. 2d, details in Methods section)^{7,44,45,48}. Our analysis demonstrates that there are four states of molecular rearrangement upon photoperturbation, populated with time constants τ_{early} , τ_{mid} , and τ_{late} . The time intervals in which the three observed processes take place are very narrow for the ten homologs we investigated, evidencing that not only the structure and function of MCL-1 are conserved across a wide and diverse range of today's living animals (Fig. 1) but also the underlying protein dynamics (Fig. 2e). This stands in stark contrast to the significant alterations that we observe for the primary structure of the protein homologs (Fig. 1c). When we plot the time constants against an evolutionary time scale (Fig. 2f), we find that the processes populated with τ_{mid} , correlate with the evolutionary divergence. In contrast, we did not detect similar protein dynamic drifts for the other two time constants, showing an absence of correlation of early- and late protein response with evolutionary divergence. On the other hand, if the time constants are plotted in dependence of the experimental binding affinities, it becomes evident that the processes populated with τ_{late} are strongly correlated with the protein's affinity (Fig. 2g).

We specified which parts of the protein complex contribute to which process by recording kinetic footprints for ¹³C-¹⁵N-labelled MCL-1 of *M. musculus* in complex with non-labelled PUMA BH3 (Extended Data Fig. 5). Separating in this way the protein from the peptide response, we found that time constant τ_{early} (= 0.9-3.5 ns) can be attributed to the α -helical unfolding of the PUMA BH3 peptide. (Fig. 2h) The time constant τ_{mid} (= 21-50 ns) corresponds to spectral features which shift ≈ 50 cm^{-1} for isotope labelled MCL-1 (Extended Data Fig. 5), and can thus be traced back to a initial response of MCL-1, that potentially allows to rearrange and cope with the conformational destabilization originating from the binding pocket. Apparently, mammalian homologs exhibit an earlier MCL-1 adaption upon destabilization than non-mammalian/vertebrate species and again other non-vertebrata (Fig. 2f, red). Finally, the terminal time constant τ_{late} (= 0.7-3.6 μ s) corresponds to mutual re-

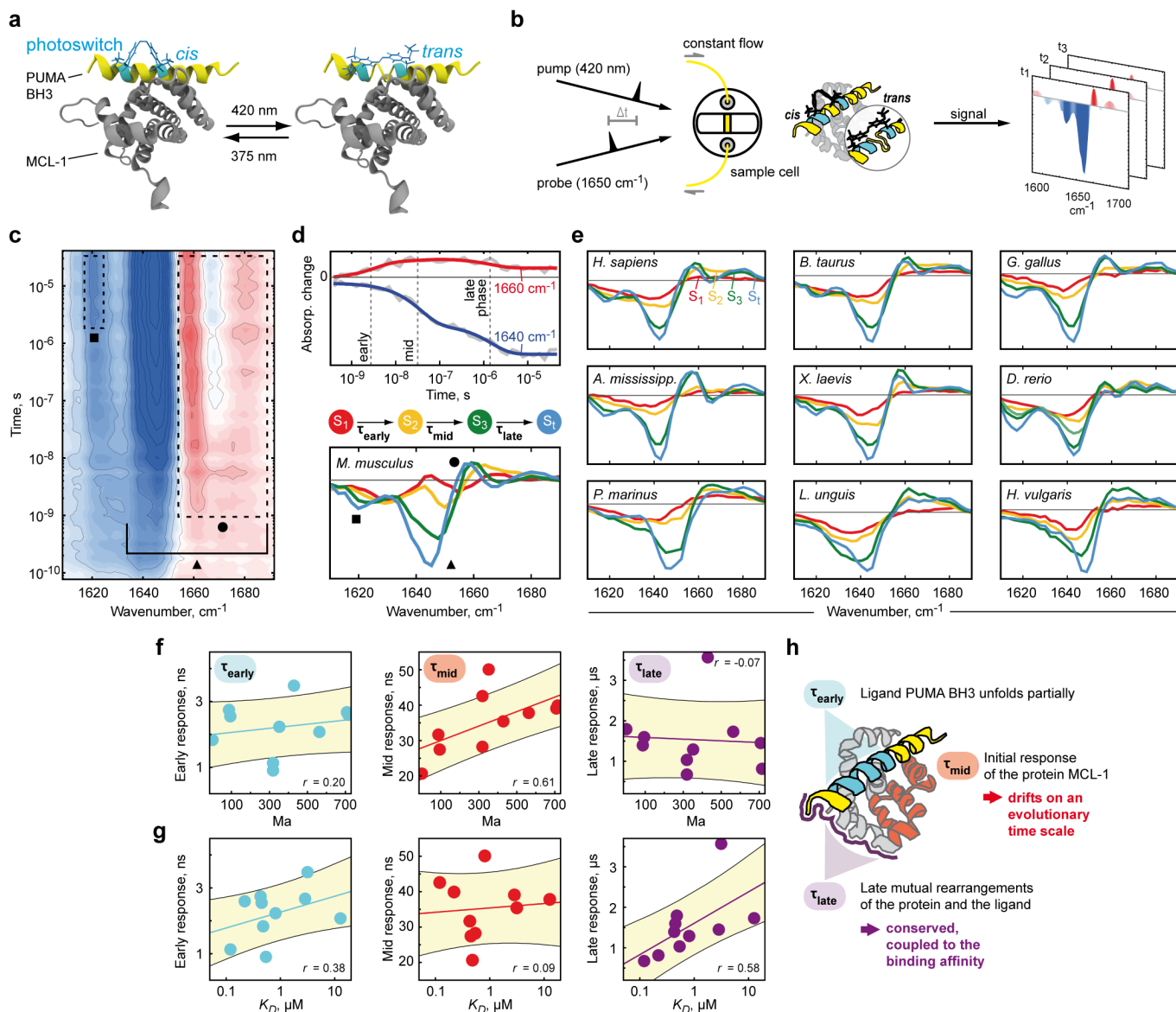


FIG. 2. The conservation of ultrafast protein dynamics in MCL-1. (a) The protein MCL-1 in complex with the photoswitchable PUMA BH3 peptide. (b) Transient infrared spectroscopy of the photo-perturbed MCL-1/PUMA BH3 complex results in kinetic footprints for all homologs, exemplarily displayed in (c) for *Mus musculus*. The symbols serve as reference points for explanations in the main text. (d) Three dominating phases of increased dynamic activity are assessed (early-, mid-, late phase; dashed lines). Global multiexponential fitting with three time constants yields fits (red/blue) that cover the raw data (grey) well. Evolution-associated difference spectra^{44,45} (lower panel) were calculated for state S₁ (red), S₂ (yellow), S₃ (green), and for S_t (blue) with time constants τ_{early} , τ_{mid} , and τ_{late} . (e) The difference spectra of all homologs display a high degree of similarity. (f) Time constants of increased dynamic activity τ_{early} , τ_{mid} , and τ_{late} against evolutionary divergence in million years, Ma. (g) Time constants τ_{early} , τ_{mid} , and τ_{late} against MCL-1's affinity for PUMA BH3. Data in (f) and (g) are displayed with linear fits \pm standard deviation (yellow) and correlation coefficients r (Pearson). (h) Isotope labeling (Extended Data Fig. 5) helped to separate the signal contribution of MCL-1 and PUMA BH3 spatially and temporally. The time constants were assigned to dynamic processes in the protein complex (schematic overview).

arrangements in the whole complex. The results are in line with previous observations for the isotope labelled human MCL-1/BIM complex⁷.

From our results, one might speculate whether MCL-1's initial response (τ_{mid}) has met with less selective pressure in the past, causing it to drift. This hypoth-

esis is supported by the absence of any discernible correlation between τ_{mid} and the protein affinity (Fig. 2g), implying that the function of the protein is seemingly not entangled with this dynamic process. In contrast, a robust correlation between τ_{late} and the K_D (Fig. 2g) indicates that the late mutual rearrangements of MCL-1

and PUMA BH3 (in the microsecond regime) are connected to the function of the protein. From our observations, it seems that the relationship between the late dynamic response and the protein affinity is conserved and cannot be inferred from the evolutionary separation of species; other factors must be at play. Irrespective of how to evaluate the given correlations, what remains truly remarkable is that our results provide an unprecedented opportunity to gain insights into the speed and extent of the impact of evolution on dynamical processes.

CONCLUSION

MCL-1 is a critical player in apoptosis²⁹, not only in human beings but also in a great variety of animals³⁰. By experimentally studying ten MCL-1 homologs and their interactions with a photo-switchable ligand PUMA BH3, we gained valuable insights into the dynamics of the proteins on a broader evolutionary time scale. Using time-resolved infrared spectroscopy, we successfully recorded the kinetic footprints of the MCL-1/PUMA BH3 complex and analytically compared them – similar to bones, skulls, and footprints in the classic field of paleontology^{49,50}, or protein structures and genetic information in its molecular form^{51–53}.

Our findings reveal a remarkable degree of conservation for the protein dynamics across the homologs, highlighting the importance of these processes in preserving their anti-apoptotic function over a span of nearly a billion years. Of particular interest is the correlation we observed between one of these ultrafast processes and the evolutionary divergence among the protein homologs, a drift in protein dynamics in the nanosecond range. This discovery challenges the prevailing focus on resolving protein structures²² and dynamics in equilibrium¹⁶ or analyzing genomic data⁵³ to understand evolution. Instead, our work highlights the importance of considering nanosecond protein dynamics as a crucial factor in unraveling the evolutionary history of these proteins. With this approach, we build a bridge between the shortest (1 ns = 10^{-9} s) and the largest conceivable timescales in living matter (300 Ma $\approx 10^{16}$ s).

Overall, our study defines a starting point for exploring the dynamics of countless other proteins with varying degrees of conservation. By investigating different systems that are more or less conserved, we can gain valuable insights into the extent of evolution’s impact on nanosecond processes, and how these rapid processes translate to slow-paced protein function.

METHODS

Phylogeny and Bioinformatics

From the countless species in the tree of life we chose ten MCL-1 homolog sequences (Fig. 1b). Alongside the

Homo sapiens homolog, our selection encompasses a variety of species, including mammalian (*Mus musculus*, *Bos taurus*), avian (*Gallus gallus*), reptile (*Alligator mississippiensis*), amphibian (*Xenopus laevis*), bony fish (*Danio rerio*), and other farther related eumetazoan homologs (*Petromyzon marinus*, *Lingula unguis*). Notably, we also incorporated a homolog from *Hydra vulgaris*, one of the most distantly related organisms known to exhibit BCL-2 regulated apoptosis³⁵. The curated selection represents species whose last common ancestors existed at quasi-equidistant intervals spanning nearly a billion years of evolutionary history.

To assemble our dataset, we accessed amino acid sequences from the Uniprot database. All entries shared the common identifier “MCL-1” in their title or description. The amino acid sequence for *P. marinus* was added to the selection with the help of Jeramiah Smith (gene on Chr52: 9161036..9167581, + strand; annotated: PMZ_0059412-RA)³⁸. The sequences were aligned to the human variant (soluble domain, Δ N- Δ C aa 171–327³³) and harmonized in length (≈ 150 -160 aa) (Extended Data Fig. 1a). The chosen sequences (refer to Extended Data Tab. I) were initially controlled for by predicting their structure using AlphaFold and RosettaFold (see below) and aligning them with experimental structures from *Homo sapiens* and *Mus musculus*. From the sequences, we generated a multiple sequence alignment using Clustal Omega (EMBL-EBI)⁵⁴ (Fig. 1a).

The phylogeny in Fig. 1b was obtained from the *TimeTree* database (<http://timetree.org>)⁵. It was not computed from the investigated MCL-1 sequences. In contrast, the given phylogeny was constructed from median and adjusted divergence times which were estimated by *TimeTree* based on values from an abundance of published studies. The divergence times, always related to *H. sapiens* and tabulated in Extended Data Tab. I alongside their corresponding confidence interval, reflect the most current scientific understanding (June 2023). In figures Fig. 1c-f, and Fig. 2f, the divergence time is given in million years, Ma.

The experimental structures of MCL-1/PUMA were retrieved from PDB (*Mus musculus*: 2ROC; *Homo sapiens*: 6QFM). In addition, we predicted the structures of all MLC-1 homologs with AlphaFold²⁷ and RosettaFold²⁸. We used ColabFold⁵⁵ to generate AlphaFold-predicted structures, and the Robetta server²⁸ for RosettaFold-predicted structures, both with default parameters. To estimate the structural similarity between all protein pairs, we performed an all-against-all alignment of the predicted structures and computed the TM score and root-mean-square deviation (RMSD) of each protein pair using TM-align⁴¹. For both AlphaFold and RosettaFold, we selected the top ranked structure out of the five predictions for downstream analyses. We evaluated the quality of the predicted structure using AlphaFold predicted local distance difference test (pLDDT), a per-residue confidence metric which estimates how well the predicted structure would match

with an experimental one and which has been shown to be well-calibrated²⁷. All our predicted structures have high average pLDDT values, ranging from 0.83 to 0.93, indicating good quality predictions.

Protein preparation

Examining protein function and dynamics, we expressed ten different MCL-1 homologs using a *Escherichia coli* BL21 expression strain (Fig. 2a). Initially, the bacterial cells were transformed with a pET-30a(+) plasmid containing the corresponding MCL-1 homolog gene, using electroporation. Positive clones were selected through Kanamycin resistance. For standard expression, bacterial cultures were cultivated in lysogeny broth medium until reaching an optical density of $OD_{600} = 0.6$. The expression was induced by adding 700 μ M IPTG, followed by incubation at 30 °C for 20 hours. Cell harvest was carried out through centrifugation (3000 xg). In order to generate heavy, uniformly ¹³C/¹⁵N-labeled MCL-1, bacterial cultures were grown in minimal medium supplemented with solely heavy carbon and nitrogen sources. The cells were cultivated to an OD_{600} of 0.6, induced with 1 mM IPTG, and then further incubated at 30 °C. The expression was stopped after 4 hours with cell harvest as described above. Cell lysis was achieved by subjecting the harvested cells to sonication (20 kHz, 4 x 1 min pulses). The lysed cell suspension was purified using Ni-affinity chromatography and a His₆-Tag located at the N-terminus of the protein. Purification was carried out under native conditions. The N-terminal His₆-Tag was removed by 3C protease cleavage. Throughout this study, all analytical procedures were performed in a sample buffer composed of 50 mM Tris (pH 8) and 125 mM NaCl. Mass spectrometry was used to assess the protein’s integrity and sample purity. For long-term storage, the samples were kept at -80 °C. In total, we could express the homologs of ten species given in the main text (Extended Data Fig. 6). Under identical conditions, however, we could not express *Ornithorhynchus anatinus*, *Orchesella cincta*, and *Acanthaster planci* homologs at adequate concentrations.

Peptide preparation

PUMA BH3 (EEQWAREIGAQLRCMADDLNCQY-ERV) was synthesized using solid-state peptide synthesis on a Liberty 1 peptide synthesizer (CEM corporation, Matthews, NC, USA). In this study, the peptide was deliberately modified by introducing two mutations – replacing Arg143 and Ala150 with Cys residues – compared to the native mammalian version. These Cys residues were incorporated distal to the hydrophobic binding interface, to enable the covalent linkage of a photoswitchable azobenzene moiety. To achieve this linkage, the watersoluble photoswitch (3,3’-bis(sulfonato)-

4,4’-bis(chloroacetamido)azobenzene)⁵⁶ and the peptide with reduced Cys residues were together incubated in a 20 mM Tris (pH 8.5) at a temperature of 50 °C, under continuous stirring for a duration of 20 hours. Hereafter, the reaction product underwent purification using both anion exchange and reversed-phase chromatography (C18 10 μ m) to isolate the successfully linked peptide. For final preparation, the buffer of the isolated linked peptide was exchanged through dialysis against the sample buffer (50 mM Tris pH 8, 125 mM NaCl). The linkage’s success, as well as the peptide’s purity and integrity, were controlled via mass spectrometry.

Circular dichroism spectroscopy

The expressed MCL-1 homologs have in common that they contain eight α -helical elements³³, and exhibit a circular dichroism spectrum that is typical for α -helical structures (Extended Data Fig. 2b, yellow). In contrast, their peptide ligand PUMA BH3 is intrinsically disordered in isolation⁵⁷ (Extended Data Fig. 2b, grey). When in complex with MCL-1, PUMA BH3 assumes an α -helical shape (Extended Data Fig. 2b, black).

We utilize circular dichroism spectroscopy to accomplish two distinct objectives: (i) to evaluate the α -helical content of the MCL-1 and PUMA BH3 complex at a constant concentration, thereby assessing whether they are correctly folded, and (ii) to generate binding curves and determine dissociation constants (K_D) for all analyzed MCL-1 homologs. To record binding curves and assess the K_D values, we exploited the nature of PUMA BH3 which is intrinsically disordered in solution and only exhibits an α -helical secondary structure when bound by MCL-1’s binding groove. Hence, for an increasing concentration of bound PUMA BH3, and a constant concentration of MCL-1, the α -helical content added by titration reflects the fraction of bound peptide.

For the first aspect (i), a quartz glass cuvette with a 1 mm path length was employed, and the sample concentration was maintained at 20 μ M. We measured the spectrum between 200-260 nm at room temperature. Hereby, we examined the α -helical content of the MCL-1 and PUMA BH3 complex which served as a control to for their correct structural conformation (displayed in Extended Data Fig. 2b).

For the second aspect (ii), MCL-1 was brought to a concentration of 2 μ M. A quartz glass cuvette with a path length of 1 cm was used, and continuous stirring was maintained during the spectroscopic measurements at room temperature. To record the binding curves, we titrated both the linked and unlinked forms of the PUMA BH3 peptide to the MCL-1 homolog, offering a comprehensive understanding of the binding affinity of photoswitchable and non-photoswitchable complexes. The circular dichroism was recorded at 222 nm as a function of increasing PUMA BH3 concentration. In both scenarios (i) and (ii), measurements involving the photoswitch-

able PUMA BH3 were conducted for both the *cis*-state (achieved through illumination with a 375 nm laser) and the dark-adapted *trans*-state.

By recording the α -helical content at 222 nm as a function of increasing PUMA BH3 concentration, we received binding curves for all MCL-1 homologs. In order to calculate the dissociation constant K_D , we fitted the data to a two-state binding equilibrium^{58,59}:

$$K_D = \frac{([M] - [MP]) \times ([P] - [MP])}{[MP]} \quad (1)$$

where $[M]$ is the initial concentration of the MCL-1, $[P]$ is the initial concentration of PUMA BH3 given to the solution, and $[MP]$ is the concentration of the protein-peptide complex. For a constant $[M] = 2 \mu\text{M}$ and a variable $[P]$, the fraction of bound peptide can be understood as:

$$\text{Fraction bound} = \frac{([M]+[P]+K_D) - \sqrt{([M]+[P]+K_D)^2 - 4 \times [M] \times [P]}}{2 \times [M]} \quad (2)$$

The covalently bound photoswitch in the *cis*-state stabilizes PUMA BH3 inside the binding pocket (Fig. 1a), with significantly lower K_D values for all of the homologs (Extended Data Fig. 2m). For PUMA BH3 in the *cis* state, *Homo sapiens*, *Bos taurus*, and *Alligator mississippiensis* homologs showed the highest affinities, with K_D values in the low nanomolar regime ($<10 \text{ nM}$), a region that was classified as physiological for wild type PUMA³¹. Switching the photoswitch from its *cis*- to its *trans* configuration results in a loss in α -helicity (Extended Data Fig. 2n) and in the destabilization of PUMA BH3.

Transient infrared spectroscopy

MCL-1 and PUMA BH3 were mixed in a 1:1 ratio prior to the spectroscopic experiment. To ensure high signal strength in transient infrared spectroscopy, both the protein and peptide were brought to concentrations of $600 \mu\text{M}$ each in the final sample. The overall sample volume was $800 \mu\text{L}$. Considering concentrations $>500 \mu\text{M}$, it is expected that the PUMA BH3 peptide will be predominantly bound within MCL-1's binding pocket, as illustrated in Extended Data Fig. 2. To exclude H_2O from spectroscopic experiments, the employed buffer was exchanged to a corresponding buffer containing D_2O . Stringent precautions were taken to avert H_2O contamination by preserving the sample within a nitrogen atmosphere devoid of water vapor.

For pump-probe measurements, a pair of electronically synchronized 2.5 kHz Ti:sapphire oscillator/regenerative amplifier femtosecond laser systems (Spectra Physics) were employed, offering a maximal delay of $45 \mu\text{s}$ ^{25,60}. One of these laser systems, featuring frequency-doubled pulses (420 nm , $3 \mu\text{J}$ per pulse, focused to an approximate beam diameter of $140 \mu\text{m}$ within the sample, and

stretched to $\sim 60 \text{ ps}$ to minimize sample deposition on the sample cell windows), were used to induce the *cis* to *trans*-isomerization of the photoswitch. The second laser system was applied to generate infrared probe pulses via an optical parametric amplifier (100 fs , spot size $110 \mu\text{m}$, center wavenumber 1660 cm^{-1}). To ensure a consistent sample environment, the sample was continuously circulated within a closed-cycle flow cell system. This system consisted of a reservoir and a CaF_2 cell featuring a $50 \mu\text{m}$ optical path length. Before entering the measurement cell, the sample was irradiated in a pre-illumination step using a 375 nm continuous wave diode laser (90 mW , CrystaLaser), in order to optimally prepare the sample with $>85\%$ in the *cis*-state.

Data analysis

From time resolved infrared measurements, we obtained kinetic footprints in the form of 2D data sets $d(\omega_i, t_j)$ as a function of probe frequency ω_i and pump-probe delay time t_j (Fig. 2c, Extended Data Fig. 3). For each homolog, we subjected the 2D dataset to a global multiexponential fitting⁴⁵, operating under the premise that the investigated system can be understood as interconverting discrete states with time-invariant spectra.

We employed multiexponential functions with amplitudes $a(\omega_i, \tau_k)$ and a global set of time constants τ_k for fitting the experimental data^{48,61,62}:

$$d(\omega_i, t_j) = a_0(\omega_i) - \sum_k a(\omega_i, \tau_k) e^{-t_j/\tau_k}. \quad (3)$$

The time constants τ_k were treated as free fitting parameters, with the constraint of a minimal number of exponential terms. Based on observations with similar systems^{7,32} we excluded data before 300 ps , to prevent the influence of the pump pulse (60 ps pulse length), which results in a strong "heat signal" at 100 ps , induced by azobenzene photoisomerization, which can be universally observed for this kind of experiment^{7,24,32}. Three time constants τ_{early} , τ_{mid} , and τ_{late} were needed to adequately fit the data, dissecting the dynamic response in an early-, mid-, and late phase (Extended Data Tab. II). The one exception is *D. rerio*, which required a fourth time constant $\tau_{D.\text{rerio}} = 300 \text{ ns}$ to adequately fit the data.

Under the assumption of a sequential, unidirectional process with four states S_1, S_2, S_3, S_t and three time constants $\tau_{\text{early}}, \tau_{\text{mid}}, \tau_{\text{late}}$ connecting them, we calculated concentration profiles for each state as well the corresponding evolution-associated difference spectra⁴⁴, which are depicted in Fig. 2d,e. Commencing with state S_1 , all subsequent evolution-associated difference spectra exhibited a blue shift from 1645 cm^{-1} to around 1675 cm^{-1} . Equally to our observations for the raw data, a very distinct positive feature at 1660 cm^{-1} was detected in the evolution-associated difference spectra of the latest two states (Fig. 2d,e, green and blue).

With the help of isotope labeling⁶³ (Fig. 5), we could assign this distinct spectral maximum, populated with τ_{mid} , to the initial response of MCL-1 upon photodestabilization of its ligand. The early response at τ_{early} exclusively originates from the unfolding of PUMA BH3. The terminal, late response at τ_{late} results from mutual, heterogeneous rearrangements in MCL-1 and PUMA BH3.

ABBREVIATIONS

BH3, BCL-2 Homology Domain 3; MCL-1, Myeloid Cell Leukemia 1.

END NOTES

Acknowledgements We thank Markus B. Glutz for the synthesis of the peptide and Serge Chesnov from Functional Genomics Center Zurich for their work on the mass spectrometry and amino-acid analysis. We thank Jeremiah Smith, University of Kentucky, who provided us with the sequence of the *Petromyzon marinus*. The work has been supported by the Swiss National Science Foundation (SNF) through the Sinergia grant CRSII5_213507.

Author contributions P.J.H conceived the study. P.J.H. selected homologs and gathered sequence information, performed microbiological work, protein expression and purification, azobenzene crosslinking, and the purification of the crosslinked peptide. P.J.H. performed binding studies with circular dichroism spectroscopy. J.R. and P.J.H performed time-resolved infrared spectroscopic measurements. C.R. performed structure predictions and computed structural similarity for the homologs. P.H. conceived and built the experimental pump probe setup. P.H. developed the analysis tools for the experimental data evaluation. P.J.H. analysed the experimental data, with input from P.H. and J.R.. P.H. supervised the project and acquired the funding. P.J.H. prepared the figures. P.J.H. wrote the manuscript with strong contribution from P.H. and minor contribution from all other authors.

Competing interests

The authors declare no competing financial interest.

Additional Information

Correspondence and requests for materials should be addressed to Philipp J. Heckmeier.

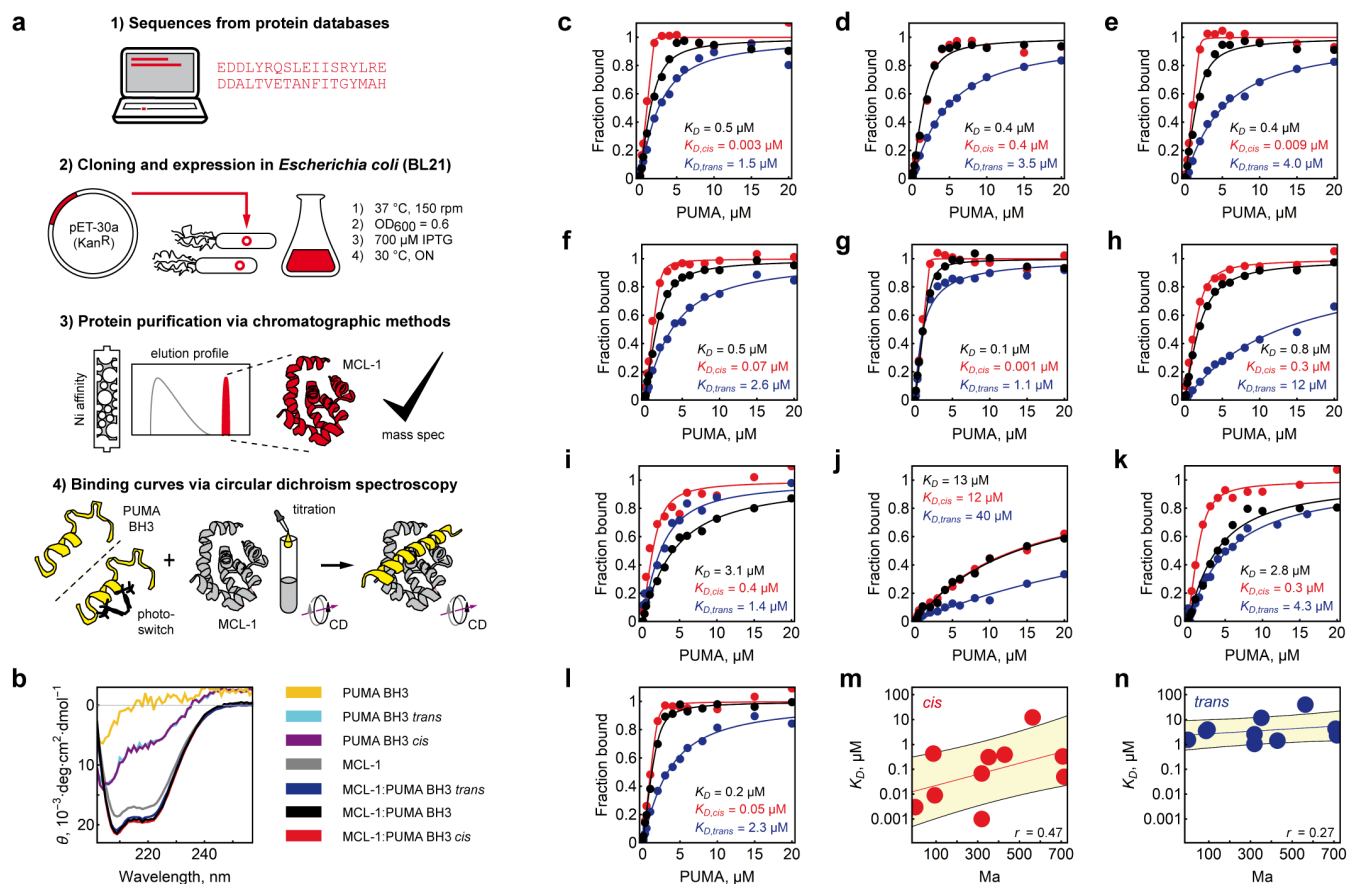
Data Availability: The data that support the findings of this study are openly available in Zenodo (the link will be provided at the proof stage.)

REFERENCES

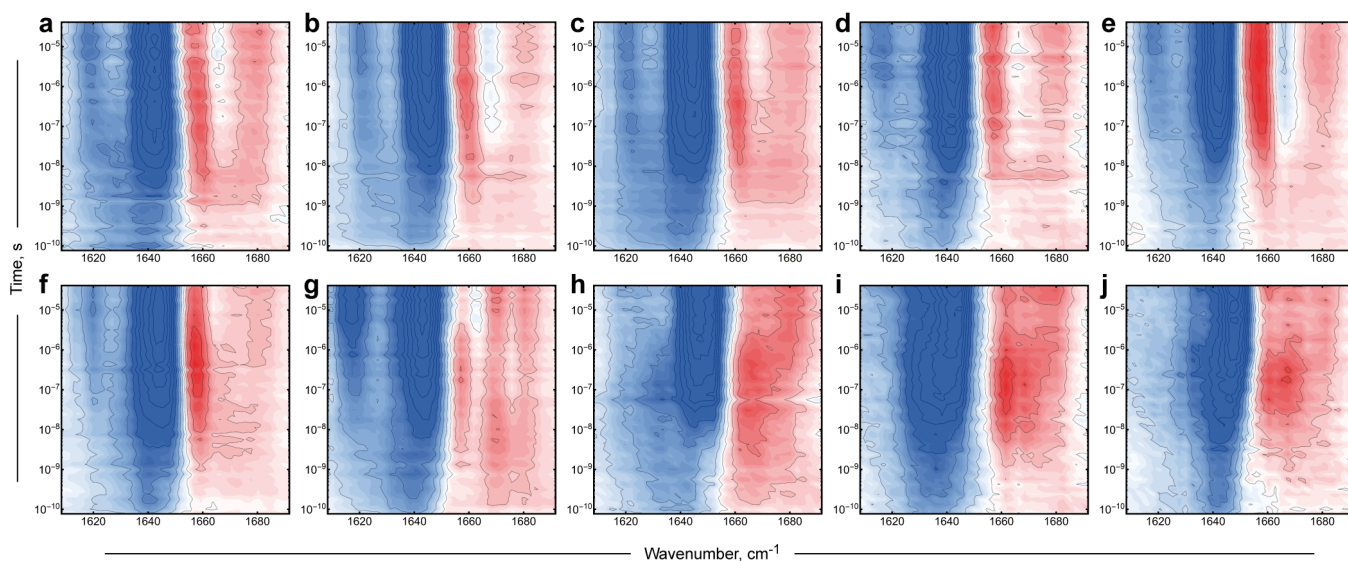
- (1) M. Karplus and J. Kuriyan, Molecular dynamics and protein function, *Proceedings of the National Academy of Sciences* **102**, 6679 (2005).
- (2) D. D. Boehr, R. Nussinov, and P. E. Wright, The role of dynamic conformational ensembles in biomolecular recognition, *Nature Chemical Biology* **5**, 789 (2009).
- (3) J. M. Adams and S. Cory, The Bcl-2 apoptotic switch in cancer development and therapy, *Oncogene* **26**, 1324 (2007).
- (4) V. Sora and E. Papaleo, Structural Details of BH3 Motifs and BH3-Mediated Interactions: an Updated Perspective, *Frontiers in Molecular Biosciences* **9**, 1 (2022).
- (5) S. Kumar, M. Suleski, J. M. Craig, A. E. Kasprowitz, M. Sanderford, M. Li, G. Stecher, and S. B. Hedges, TimeTree 5: An Expanded Resource for Species Divergence Times, *Molecular Biology and Evolution* **39**, 1 (2022).
- (6) B. Jankovic, J. Ruf, C. Zanobini, O. Bozovic, D. Buhrke, and P. Hamm, Sequence of Events during Peptide Unbinding from RNase S: A Complete Experimental Description, *Journal of Physical Chemistry Letters* **12**, 5201 (2021), 2103.13053.
- (7) P. J. Heckmeier, J. Ruf, D. Buhrke, B. G. Janković, and P. Hamm, Signal propagation within the mcl-1/bim protein complex, *Journal of Molecular Biology* **434**, 167499 (2022).
- (8) V. A. Lórenz-Fonfría, Infrared Difference Spectroscopy of Proteins: From Bands to Bonds, *Chemical Reviews* **120**, 3466 (2020).
- (9) A. Barth, Infrared spectroscopy of proteins, *Biochimica et Biophysica Acta - Bioenergetics* **1767**, 1073 (2007).
- (10) N. Galvanetto, M. T. Ivanović, A. Chowdhury, A. Sottini, M. F. Nüesch, D. Nettels, R. B. Best, and B. Schuler, Extreme dynamics in a biomolecular condensate, *Nature* **25**, 10.1038/s41586-023-06329-5 (2023).
- (11) P. Schanda and B. Brutscher, Very fast two-dimensional NMR spectroscopy for real-time investigation of dynamic events in proteins on the time scale of seconds, *Journal of the American Chemical Society* **127**, 8014 (2005).
- (12) M. Pirchi, G. Ziv, I. Riven, S. S. Cohen, N. Zohar, Y. Barak, and G. Haran, Single-molecule fluorescence spectroscopy maps the folding landscape of a large protein, *Nature Communications* **2**, 2 (2011).
- (13) H. Y. Aviram, M. Pirchi, H. Mazal, Y. Barak, I. Riven, and G. Haran, Direct observation of ultrafast large-scale dynamics of an enzyme under turnover conditions, *Proceedings of the National Academy of Sciences of the United States of America* **115**, 3243 (2018).
- (14) H. Hofmann, F. Hillger, S. H. Pfeil, A. Hoffmann, D. Streich, D. Haenni, D. Nettels, E. A. Lipman, and B. Schuler, Single-molecule spectroscopy of protein folding in a chaperonin cage, *Proceedings of the National Academy of Sciences of the United States of America* **107**, 11793 (2010).
- (15) A. Borgia, M. B. Borgia, K. Bugge, V. M. Kissling, P. O. Heidarsson, C. B. Fernandes, A. Sottini, A. Soranno, K. J. Buholzer, D. Nettels, B. B. Kragelund, R. B. Best, and B. Schuler, Extreme disorder in an ultrahigh-affinity protein complex, *Nature* **555**, 61 (2018).
- (16) P. Jemth, E. Karlsson, B. Vögeli, B. Guzovsky, E. An-

- derrsson, G. Hultqvist, J. Dogan, P. Güntert, R. Riek, and C. N. Chi, Structure and dynamics conspire in the evolution of affinity between intrinsically disordered proteins, *Science Advances* **4**, 10.1126/sciadv.aau4130 (2018).
- (17) E. Karlsson, F. A. Sorgenfrei, E. Andersson, J. Dogan, P. Jemth, and C. N. Chi, The dynamic properties of a nuclear coactivator binding domain are evolutionarily conserved, *Communications Biology* **5**, 1 (2022).
- (18) A. Schenkmyerova, G. P. Pinto, M. Toul, M. Marek, L. Hernychova, J. Planas-Iglesias, V. Daniel Liskova, D. Pluskal, M. Vasina, S. Emond, M. Dörr, R. Chaloupkova, D. Bednar, Z. Prokop, F. Hollfelder, U. T. Bornscheuer, and J. Damborsky, Engineering the protein dynamics of an ancestral luciferase, *Nature Communications* **12**, 10.1038/s41467-021-23450-z (2021).
- (19) E. A. Ortlund, J. T. Bridgham, M. R. Redinbo, and J. W. Thornton, Crystal Structure of an Ancient Protein: Evolution by Conformational Epistasis, *Science* **317**, 1544 (2007).
- (20) A. Ingles-Prieto, B. Ibarra-Molero, A. Delgado-Delgado, R. Perez-Jimenez, J. M. Fernandez, E. A. Gaucher, J. M. Sanchez-Ruiz, and J. A. Gavira, Conservation of protein structure over four billion years, *Structure* **21**, 1690 (2013).
- (21) V. Nguyen, C. Wilson, M. Hoemberger, J. B. Stiller, R. V. Agafonov, S. Kutter, J. English, D. L. Theobald, and D. Kern, Evolutionary drivers of thermoadaptation in enzyme catalysis, *Science* **355**, 289 (2017).
- (22) A. Hadzipasic, C. Wilson, V. Nguyen, N. Kern, C. Kim, W. Pitsawong, J. Villali, Y. Zheng, and D. Kern, Ancient origins of allosteric activation in a Ser-Thr kinase, *Science* **367**, 912 (2020).
- (23) T. R. Alderson and L. E. Kay, NMR spectroscopy captures the essential role of dynamics in regulating biomolecular function, *Cell* **184**, 577 (2021).
- (24) O. Bozovic, C. Zanobini, A. Gulzar, B. Jankovic, D. Buhrke, M. Post, S. Wolf, G. Stock, and P. Hamm, Real-time observation of ligand-induced allosteric transitions in a PDZ domain, *Proceedings of the National Academy of Sciences of the United States of America* **117**, 26031 (2020).
- (25) J. Helbing and P. Hamm, Versatile Femtosecond Laser Synchronization for Multiple-Timescale Transient Infrared Spectroscopy, *The Journal of Physical Chemistry A* **127**, 6347 (2023), 2305.14747.
- (26) C. L. Day, C. Smits, F. C. Fan, E. F. Lee, W. D. Fairlie, and M. G. Hinds, Structure of the BH3 Domains from the p53-Inducible BH3-Only Proteins Noxa and Puma in Complex with Mcl-1, *Journal of Molecular Biology* **380**, 958 (2008).
- (27) J. Jumper, R. Evans, A. Pritzel, T. Green, M. Figurnov, O. Ronneberger, K. Tunyasuvunakool, R. Bates, A. Židek, A. Potapenko, A. Bridgland, C. Meyer, S. A. Kohl, A. J. Ballard, A. Cowie, B. Romera-Paredes, S. Nikolov, R. Jain, J. Adler, T. Back, S. Petersen, D. Reiman, E. Clancy, M. Zielinski, M. Steinegger, M. Pacholska, T. Berghammer, S. Bodenstein, D. Silver, O. Vinyals, A. W. Senior, K. Kavukcuoglu, P. Kohli, and D. Hassabis, Highly accurate protein structure prediction with AlphaFold, *Nature* **596**, 583 (2021).
- (28) M. Baek, F. DiMaio, I. Anishchenko, J. Dauparas, S. Ovchinnikov, G. R. Lee, J. Wang, Q. Cong, L. N. Kinch, R. Dustin Schaeffer, C. Millán, H. Park, C. Adams, C. R. Glassman, A. DeGiovanni, J. H. Pereira, A. V. Rodrigues, A. A. Van Dijk, A. C. Ebrecht, D. J. Opperman, T. Sagmeister, C. Buhlheller, T. Pavkov-Keller, M. K. Rathinaswamy, U. Dalwadi, C. K. Yip, J. E. Burke, K. Christopher Garcia, N. V. Grishin, P. D. Adams, R. J. Read, and D. Baker, Accurate prediction of protein structures and interactions using a three-track neural network, *Science* **373**, 871 (2021).
- (29) R. J. Youle and A. Strasser, The BCL-2 protein family: Opposing activities that mediate cell death, *Nature Reviews Molecular Cell Biology* **9**, 47 (2008).
- (30) A. Aouacheria, C. Combet, P. Tompa, and J. M. Hardwick, Redefining the BH3 Death Domain as a ‘Short Linear Motif’, *Trends in Biochemical Sciences* **40**, 736 (2015).
- (31) J. Kale, E. J. Osterlund, and D. W. Andrews, BCL-2 family proteins: changing partners in the dance towards death, *Cell Death and Differentiation* **25**, 65 (2018).
- (32) P. J. Heckmeier, J. Ruf, B. G. Janković, and P. Hamm, MCL-1 promiscuity and the structural resilience of its binding partners, *Journal of Chemical Physics* **158**, 10.1063/5.0137239 (2023).
- (33) P. E. Czabotar, E. F. Lee, M. F. van Delft, C. L. Day, B. J. Smith, D. C. S. Huang, W. D. Fairlie, M. G. Hinds, and P. M. Colman, Structural insights into the degradation of Mcl-1 induced by BH3 domains, *Proceedings of the National Academy of Sciences of the United States of America* **104**, 6217 (2007).
- (34) M. Wiens, B. Diehl-Seifert, and W. E. G. Müller, Sponge Bcl-2 homologous protein (BHP2-GC) confers distinct stress resistance to human HEK-293 cells, *Cell Death & Differentiation* **8**, 887 (2001).
- (35) M. Lasi, B. Pauly, N. Schmidt, M. Cikala, B. Stiening, T. Käsbauer, G. Zenner, T. Popp, A. Wagner, R. T. Knapp, A. H. Huber, M. Grunert, J. Söding, C. N. David, and A. Böttger, The molecular cell death machinery in the simple cnidarian Hydra includes an expanded caspase family and pro- and anti-apoptotic Bcl-2 proteins, *Cell Research* **20**, 812 (2010).
- (36) M. J. Harms and J. W. Thornton, Analyzing protein structure and function using ancestral gene reconstruction, *Current Opinion in Structural Biology* **20**, 360 (2010).
- (37) R. Merkl and R. Sterner, Ancestral protein reconstruction: Techniques and applications, *Biological Chemistry* **397**, 1 (2016).
- (38) N. Timoshevskaya, K. I. Eşkut, V. A. Timoshevskiy, S. M. Robb, C. Holt, J. E. Hess, H. J. Parker, C. F. Baker, A. K. Miller, C. Saraceno, M. Yandell, R. Krumlauf, S. R. Narum, R. T. Lampman, N. J. Gemmill, J. Mountcastle, B. Haase, J. R. Balacco, G. Formenti, S. Pelan, Y. Sims, K. Howe, O. Fedrigo, E. D. Jarvis, and J. J. Smith, An improved germline genome assembly for the sea lamprey *Petromyzon marinus* illuminates the evolution of germline-specific chromosomes, *Cell Reports* **42**, 112263 (2023).
- (39) W. R. Pearson, An introduction to sequence similarity (“homology”) searching, *Current Protocols in Bioinformatics* 10.1002/0471250953.bi0301s42 (2013).
- (40) A. McGriff and W. J. Placzek, Phylogenetic analysis of the MCL1 BH3 binding groove and rBH3 sequence motifs in the p53 and INK4 protein families, *PLoS ONE* **18**, 1 (2023).
- (41) Y. Zhang and J. Skolnick, TM-align: a protein struc-

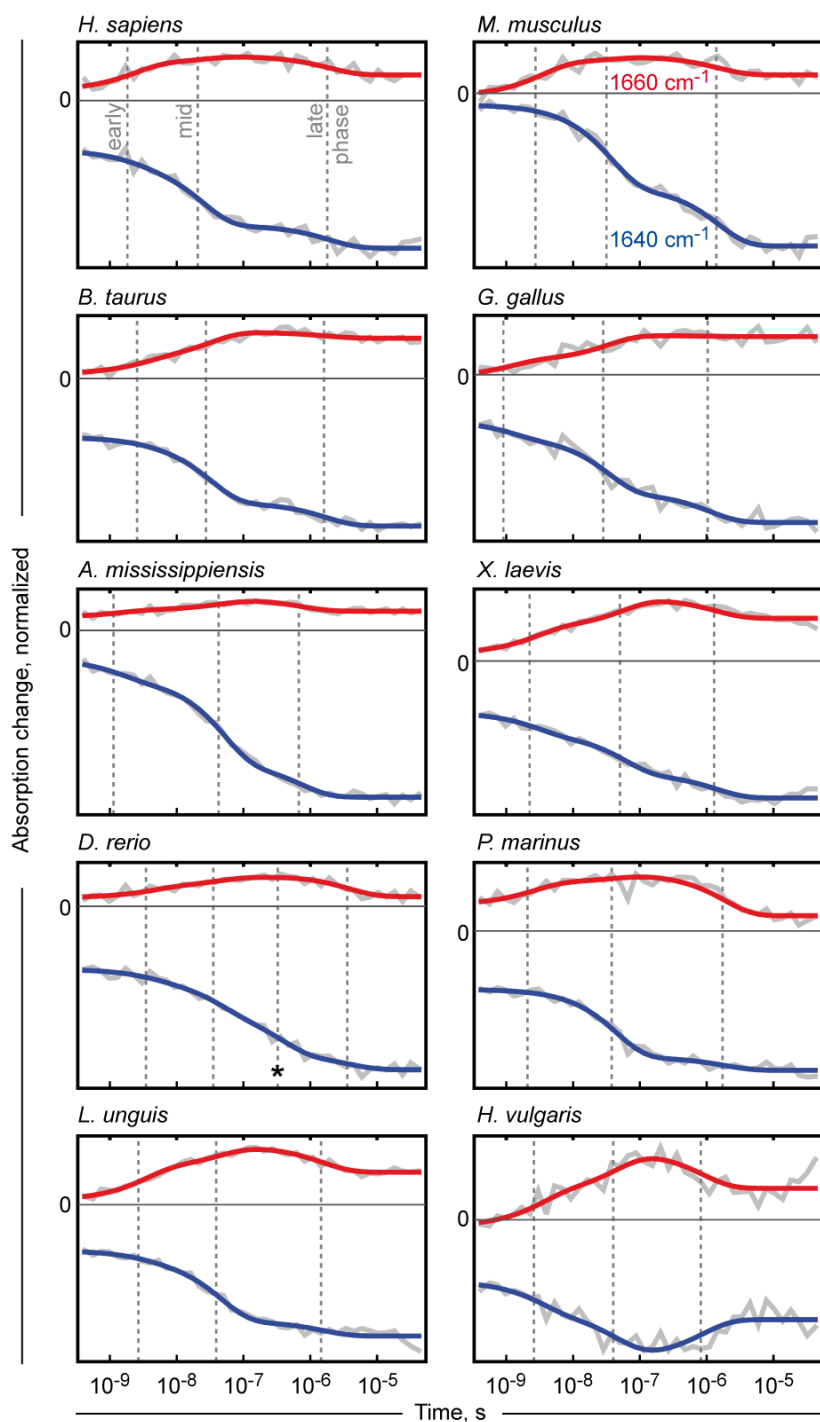
- ture alignment algorithm based on the TM-score, *Nucleic Acids Research* **33**, 2302 (2005).
- (42) J. Xu and Y. Zhang, How significant is a protein structure similarity with TM-score = 0.5?, *Bioinformatics* **26**, 889 (2010).
- (43) C. Chothia and A. Lesk, The relation between the divergence of sequence and structure in proteins., *The EMBO Journal* **5**, 823 (1986).
- (44) I. H. Van Stokkum, D. S. Larsen, and R. Van Gron-delle, Global and target analysis of time-resolved spectra, *Biochimica et Biophysica Acta - Bioenergetics* **1657**, 82 (2004).
- (45) D. Buhrke, K. T. Oppelt, P. J. Heckmeier, R. Fernández-Terán, and P. Hamm, Nanosecond protein dynamics in a red/green cyanobacteriochrome revealed by transient IR spectroscopy, *Journal of Chemical Physics* **153**, 245101 (2020).
- (46) A. Barth and C. Zscherp, What vibrations tell us about proteins, *Q. Rev. Biophys.* **35**, 369 (2002).
- (47) C. Y. Huang, Z. Getahun, Y. Zhu, J. W. Klemke, W. F. Degrado, and F. Gai, Helix formation via conformation diffusion search, *Proceedings of the National Academy of Sciences of the United States of America* **99**, 2788 (2002).
- (48) V. A. Lórenz-Fonfría and H. Kandori, Transformation of Time-Resolved Spectra to Lifetime-Resolved Spectra by Maximum Entropy Inversion of the Laplace Transform, *Applied Spectroscopy* **60**, 407 (2006).
- (49) J. T. Stern and R. L. Susman, The locomotor anatomy of *Australopithecus afarensis*, *American Journal of Physical Anthropology* **60**, 279 (1983).
- (50) P. E. Olsen, J. B. Smith, and N. G. McDonald, Type material of the type species of the classic theropod footprint genera *Eubrontes*, *Anchisauripus*, and *Grallator* (Early Jurassic, Hartford and Deerfield basins, Connecticut and Massachusetts, U.S.A.), *Journal of Vertebrate Paleontology* **18**, 586 (1998).
- (51) M.-C. King and A. C. Wilson, Evolution at Two Levels in Humans and Chimpanzees, *Science* **188**, 107 (1975).
- (52) D. Reich, R. E. Green, M. Kircher, J. Krause, N. Patterson, E. Y. Durand, B. Viola, A. W. Briggs, U. Stenzel, P. L. Johnson, T. Maricic, J. M. Good, T. Marques-Bonet, C. Alkan, Q. Fu, S. Mallick, H. Li, M. Meyer, E. E. Eichler, M. Stoneking, M. Richards, S. Talamo, M. V. Shunkov, A. P. Derevianko, J. J. Hublin, J. Kelso, M. Slatkin, and S. Pääbo, Genetic history of an archaic hominin group from Denisova cave in Siberia, *Nature* **468**, 1053 (2010).
- (53) T. van der Valk, P. Pečnerová, D. Díez-del Molino, A. Bergström, J. Oppenheimer, S. Hartmann, G. Xenikoudakis, J. A. Thomas, M. Dehasque, E. Sağlıcan, F. R. Fidan, I. Barnes, S. Liu, M. Somel, P. D. Heintzman, P. Nikolskiy, B. Shapiro, P. Skoglund, M. Hofreiter, A. M. Lister, A. Götherström, and L. Dalén, Million-year-old DNA sheds light on the genomic history of mammoths, *Nature* **591**, 265 (2021).
- (54) F. Sievers, A. Wilm, D. Dineen, T. J. Gibson, K. Karplus, W. Li, R. Lopez, H. McWilliam, M. Remmert, J. Söding, J. D. Thompson, and D. G. Higgins, Fast, scalable generation of high-quality protein multiple sequence alignments using Clustal Omega, *Molecular Systems Biology* **7**, 10.1038/msb.2011.75 (2011).
- (55) M. Mirdita, K. Schütze, Y. Moriwaki, L. Heo, S. Ovchinnikov, and M. Steinegger, Colabfold: making protein folding accessible to all, *Nature methods* **19**, 679 (2022).
- (56) Z. Zhang, D. C. Burns, J. R. Kumita, O. S. Smart, and G. A. Woolley, A Water-Soluble Azobenzene Cross-Linker for Photocontrol of Peptide Conformation, *Bioconjugate Chemistry* **14**, 824 (2003).
- (57) M. G. Hinds, C. Smits, R. Fredericks-Short, J. M. Risk, M. Bailey, D. C. S. Huang, and C. L. Day, Bim, Bad and Bmf: intrinsically unstructured BH3-only proteins that undergo a localized conformational change upon binding to pro-survival Bcl-2 targets, *Cell Death and Differentiation* **14**, 128 (2007).
- (58) B. Jankovic, A. Gulzar, C. Zanobini, O. Bozovic, S. Wolf, G. Stock, and P. Hamm, Photocontrolling Protein–Peptide Interactions: From Minimal Perturbation to Complete Unbinding, *Journal of the American Chemical Society* **141**, 10702 (2019).
- (59) I. Jarmoskaite, I. Alsdhan, P. P. Vaidyanathan, and D. Herschlag, How to measure and evaluate binding affinities, *eLife* **9**, 1 (2020).
- (60) J. Bredenbeck, J. Helbing, and P. Hamm, Continuous scanning from picoseconds to microseconds in time resolved linear and nonlinear spectroscopy, *Review of Scientific Instruments* **75**, 4462 (2004).
- (61) M. P. Hobson and A. N. Lasenby, The entropic prior for distributions with positive and negative values, *Monthly Notices of the Royal Astronomical Society* **298**, 905 (1998).
- (62) A. T. N. Kumar, L. Zhu, J. F. Christian, A. A. Demidov, and P. M. Champion, On the Rate Distribution Analysis of Kinetic Data Using the Maximum Entropy Method: Applications to Myoglobin Relaxation on the Nanosecond and Femtosecond Timescales, *The Journal of Physical Chemistry B* **105**, 7847 (2001).
- (63) P. I. Haris, D. Chapman, G. T. Robillard, and A. A. van Dijk, Potential of carbon-13 and nitrogen-15 labeling for studying protein-protein interactions using Fourier-transform infrared spectroscopy, *Biochemistry* **31**, 6279 (1992).



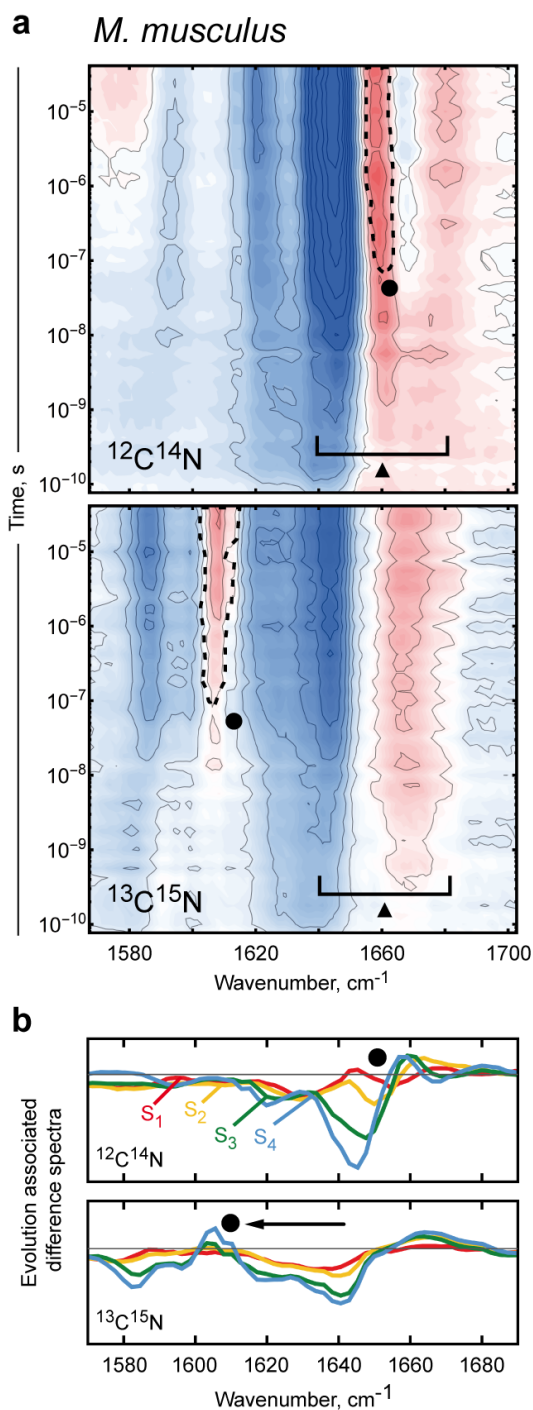
Extended Data Fig. 2. The binding affinities of ten MCL-1 homologs. (a) Generation of ten MCL-1 homologs for spectroscopic experiments. (b) Circular dichroism spectroscopy of the MCL-1/PUMA BH3 complex. PUMA BH3 is intrinsically disordered and only assumes an α -helical shape when bound to MCL-1. When linked to an azobenzene photoswitch, PUMA BH3 is destabilized in the *trans*-state of the photoswitch moiety. Binding curves for (c) *Homo sapiens*, (d) *Mus musculus*, (e) *Bos taurus*, (f) *Gallus gallus*, (g) *Alligator mississippiensis*, (h) *Xenopus laevis*, (i) *Danio rerio*, (j) *Petromyzon marinus*, (k) *Lingula unguis*, and (l) *Hydra vulgaris*. The binding affinity in *cis*-state (m) and *trans*-state against the evolutionary divergence in million years, Ma. Yellow, linear fit \pm standard deviation; plots are displayed with the Pearson correlation coefficient r .



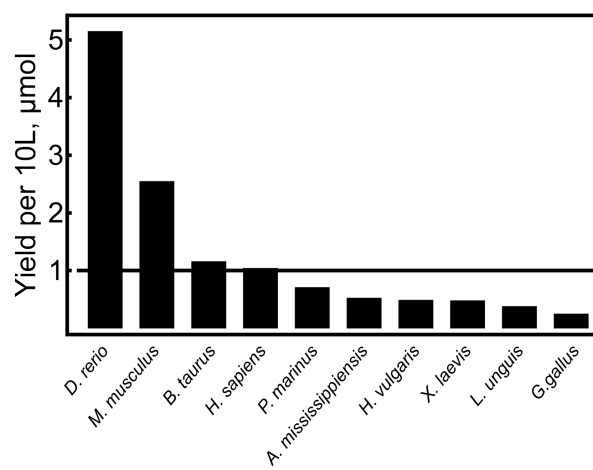
Extended Data Fig. 3. Kinetic responses, serving as footprints, for (a) *Homo sapiens*, (b) *Mus musculus* (divergence time: 87 million years, Ma), (c) *Bos taurus* (94 Ma), (d) *Gallus gallus* (319 Ma), (e) *Alligator mississippiensis* (319 Ma), (f) *Xenopus laevis* (352 Ma), (g) *Danio rerio* (429 Ma), (h) *Petromyzon marinus* (563 Ma), (i) *Lingula unguis* (708 Ma), and (j) *Hydra vulgaris* (715 Ma). The kinetic footprints display comparable elements. We observe fine differences between closer related homologs and diverging, gradually emphasized features for farther related homologs, indicating an evolutionary timescale in which protein dynamic processes have changed.



Extended Data Fig. 4. The dynamic response upon photo-perturbation can be subdivided into an early-, mid-, and late phase, exemplified here for kinetic traces at 1640 cm^{-1} and 1660 cm^{-1} . When analyzed with global multiexponential fitting and three time constants τ_{early} , τ_{mid} , and τ_{late} (given as dashed lines), the resulting fits (red/blue) are congruent with the time traces (grey). The one exception is *D. rerio*, which requires an additional fourth time constant $\tau_{D.\text{rerio}} = 300\text{ ns}$ (*) to adequately fit the data.



Extended Data Fig. 5. Transient infrared spectroscopy with isotope labeled MCL-1/PUMA BH3 complexes. From ten homologs, *M. musculus* was chosen as a representative, as $^{13}\text{C}^{15}\text{N}$ -labeling is highly cost intensive. (a) Kinetic footprints of unlabeled samples (upper panel), and of samples with $^{13}\text{C}^{15}\text{N}$ -labeled MCL-1 (lower panel). The early protein response (triangle) is not shifted for the labeled sample. The mid protein response (circle) manifests in a distinct sharp feature that shifts from 1660 cm^{-1} to 1610 cm^{-1} upon isotope labeling (dashed lines). Isotope labeling did not separate any spectral features at the late phase of the protein response. (b) Evolution-associated difference spectra (see Data analysis in the Methods section) display a relatively sharp positive band in state S_3 and S_4 (circle). In the non-labeled complex, the sharp maximum coincides with the broad positive band of the blue shift. For the labeled complex, it is shifted by 50 cm^{-1} from 1660 cm^{-1} to 1610 cm^{-1} , as expected for $^{13}\text{C}^{15}\text{N}$ -labeling⁶³.



Extended Data Fig. 6. Expression yield of various MCL-1 homologs from 10 L *Escherichia coli* culture. A yield of 1 μmol was seen crucial for spectroscopic analysis.

Extended Data Table I. Selection of species whose MCL-1 homologs were investigated

	MCL-1 Uniprot ref. ID	divergence time, Ma	confidence interval, Ma
<i>H. sapiens</i>	Q07820	0	-
<i>M. musculus</i>	P97287	87	81-91
<i>B. taurus</i>	A5PJR2	94	92-97
<i>G. gallus</i>	(A0A1L1RNM6)* XP_046788511.1	319	316-322
<i>A. mississippiensis</i>	A0A151NDN7	319	316-322
<i>X. laevis</i>	B6V6J0	352	348-356
<i>D. rerio</i>	(Q1L8X3)** UPI000056A44D	429	423-440
<i>P. marinus</i>	-	563	494-652
<i>L. unguis</i>	A0A1S3IZP1_LINUN	708	627-830
<i>H. vulgaris</i>	A1E3K7	715	604-1250

*Uniprot entry (Dec 2022) has become obsolete. NCBI reference ID is given instead. **Uniprot entry (Dec 2022) has become obsolete. Uniparc ID is given instead.

The divergence times are related to *H. sapiens*.

Extended Data Table II. Time constants representing the early-, mid-, and late phase of the dynamic response.

	τ_{early}	τ_{mid}	τ_{late}
	ns	ns	μs
<i>H. sapiens</i>	1.8	21	1.8
<i>M. musculus</i>	2.7	31	1.4
<i>B. taurus</i>	2.5	27	1.6
<i>G. gallus</i>	0.9	28	1.0
<i>A. mississippiensis</i>	1.1	43	0.7
<i>X. laevis</i>	2.2	50	1.3
<i>D. rerio</i>	3.5	35	3.6
<i>P. marinus</i>	2.1	38	1.7
<i>L. unguis</i>	2.7	39	1.5
<i>H. vulgaris</i>	2.6	40	0.8
<i>M. musculus</i> ($^{13}C^{15}N$)	3.9	36	2.3